Determining the mode II fracture properties of a structural adhesive using the direct method

B.D. Simões (INEGI,Portugal), D.S. Correia, F. Ramezani, E.A.S. Marques, R.J.C. Carbas, L.F.M. da Silva

ADVANCED JOINING PROCESSES UNIT

Abstract

The use of structural adhesives in high-performance applications like automotive and aeronautical fields has increased, offering benefits such as weight reduction, cost savings, and emission reduction. Adhesive bonding joins dissimilar materials and ensures uniform stress distribution. In the automotive sector, they are vital for critical structural parts. However, due to their use in safety-critical structures, robust experimental and computational techniques are essential for predicting and characterizing joint behavior. This study involved experimental and numerical investigations of End-Notched Flexure (ENF) specimens to characterize the fracture behavior of a structural film adhesive in mode II. Fracture toughness and cohesive law were determined using the J-integral approach and direct method, respectively. The cohesive law was then applied to a cohesive zone model (CZM) in ABAQUS software, and numerical results were compared with experimental data.

Experimental details

Joint geometry

The specimens' geometry is presented in Figure 1. The ENF specimen, with CFRP substrates, was used to perform fracture tests and characterize the fracture behaviour of the adhesive Scotch Weld AF 163-2k supplied by 3M Company. This material is a modified epoxy in a film form with high fracture toughness and peel strength.
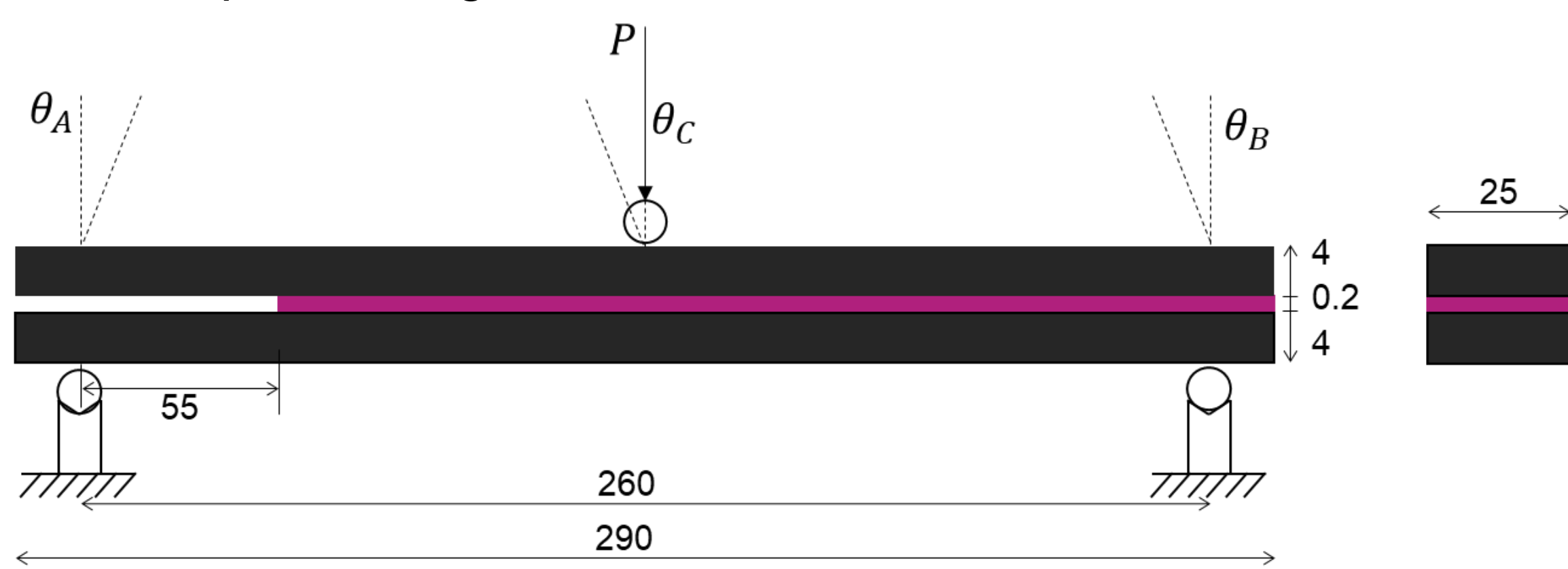
Figure 1 – Specimens' geometry, in mm.

Cohesive law (CL)

The experimental law combines fracture toughness values from the J-integral approach with CTD values. Rotations (Figure 1) were calculated using inclinometers, and CTD was determined using digital image correlation. Equations 1 and 2 represent expressions for J-integral and CL, respectively.

$$J = \frac{P}{2b} \cdot (\theta_A - 2\theta_B + \theta_B) \quad (1) \qquad \tau = \frac{J_{t+\Delta t} - J_t}{\delta_{s_{t+\Delta t}} - \delta_{s_t}} \quad (2)$$

Where P is the applied load, b is the width of the specimen, θ is the rotation of the substrate in the different points of interest, and δ_s is the CTD.

Experimental Results

Fracture energy

Figure 2 (left) displays the fracture energy results obtained using the J-integral approach. The propagation plateau averaged 8.13 N/mm, exhibiting good repeatability and stable crack propagation. The curves showed a final increase when the crack reached the middle roller of the apparatus. Figure 2 (right) illustrates that both J-integral and Compliance Based Beam Method (CBBM) approaches yielded the similar values for mode II fracture energy.
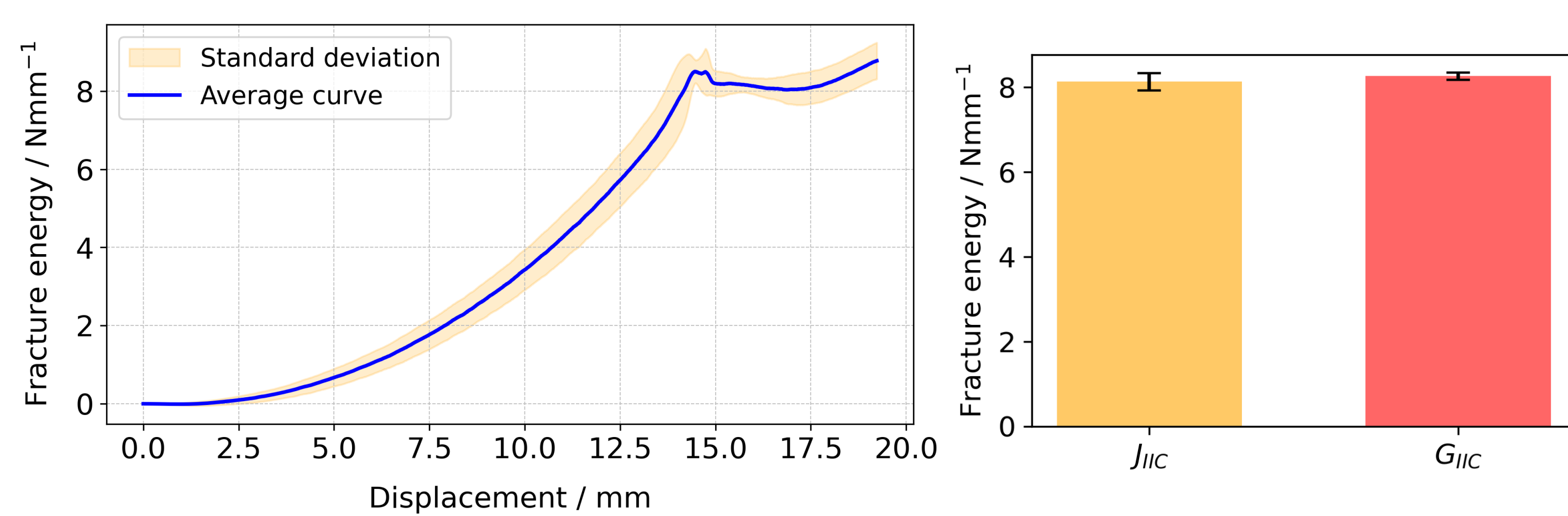
Figure 2 – Fracture energy curves obtained with J-integral (left) and comparison between J-integral and CBBM approaches (right).

Direct CL

A CZM model was developed to predict the adhesive behavior in mode II. Figure 3 (left) shows the directly obtained CL with experimental points and a smoothed line. The graded color map displays the density probability of the experimental points. Figure 3 (right) illustrates the damage variable calculated from the CL.
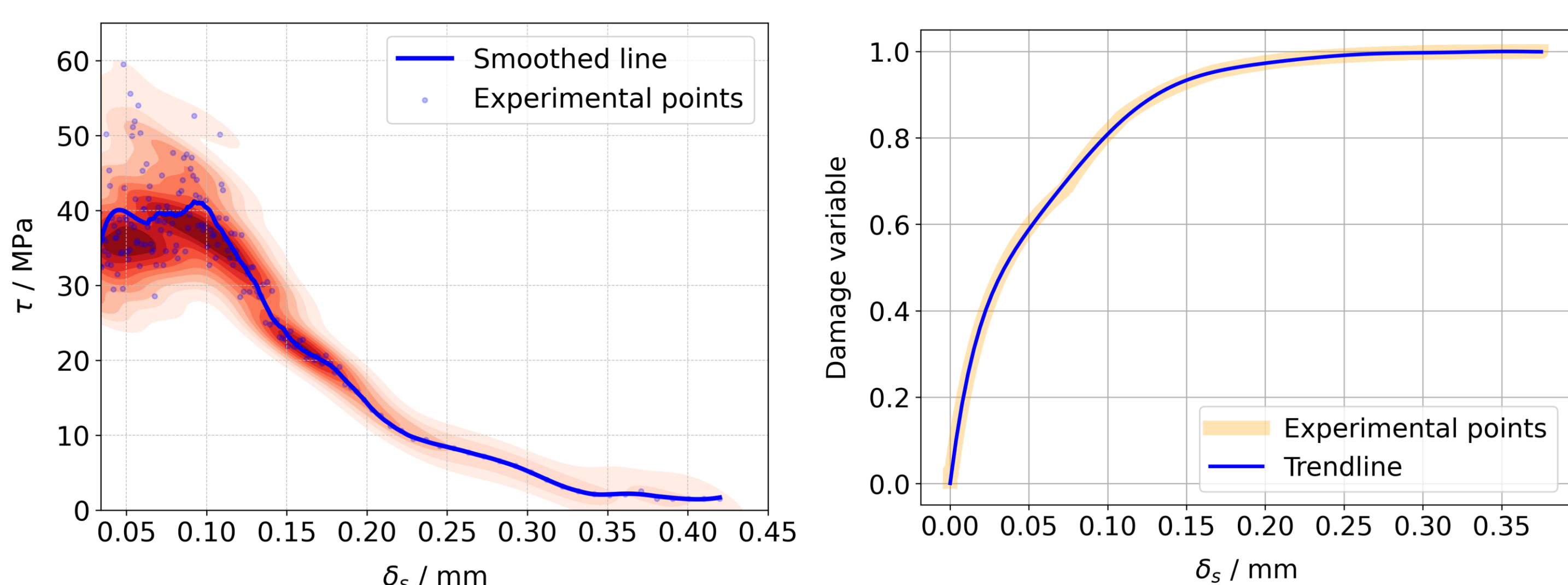
Figure 3 – Experimental CL with the experimental points, the smoothed line and the density probability map (left) and the damage variable as a function of CTD (right).

Numerical validation

Fracture process monitoring

Figure 4 displays three frames from the entire simulation, showing the evolution of the Fracture Process Zone (FPZ) from initiation (a), to propagation (b) and finally when it is beneath the roller (c). In each frame, the crack tip (red diamond) of the ENF specimen and the corresponding damaged region ahead of it (up to the blue diamond) are visible to aid FPZ visualization. This result is aligned to the experimental results, leading to an increase in fracture anergy after stable propagation.

(a) Beginning of crack propagation.   (b) Crack propagation.

(c) Crack propagation beneath the roller.
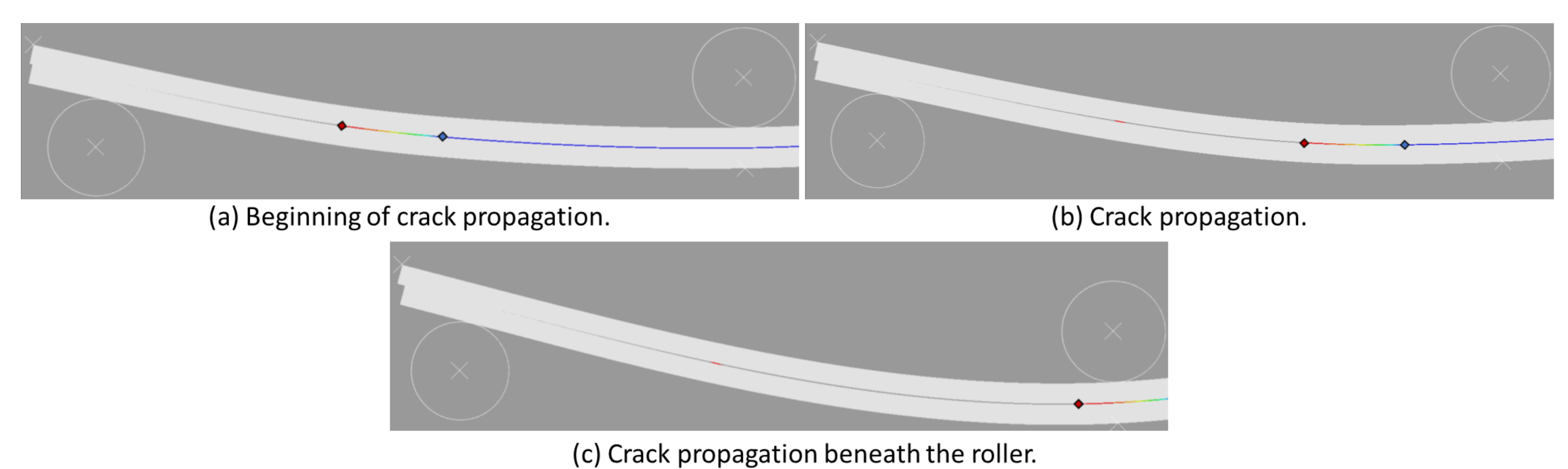
Figure 4 – FPZ evolution from initiation (a), to propagation (b) and when the crack is beneath the roller (c).

Numerical validation

Figure 5 presents the von Mises stress distribution during the ENF test, before (top) and after (bottom) crack propagation. It can be observed that the stresses in the ENF specimen are dependent on the test increment. The higher stresses move from the middle roller to the FPZ area, after the crack propagates.
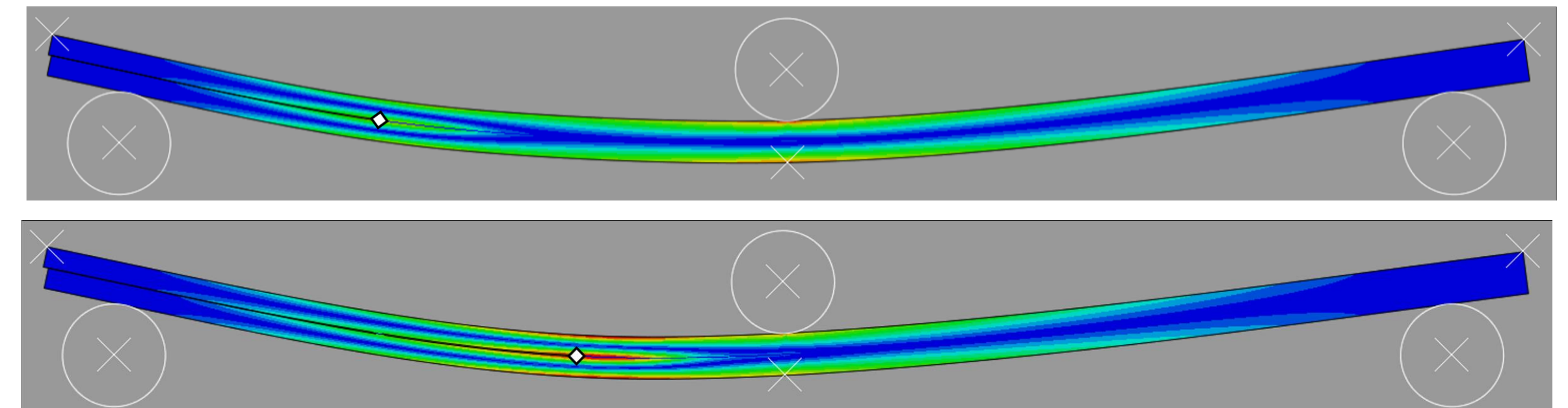
Figure 5 – Stress distribution before (top) and after (bottom) crack propagation.

The results obtained with the developed CZM model, together with the experimental data, can be depicted in Figure 6. The developed model presents an overall good prediction, although the damage after crack propagation was overestimated, resulting in lower load values.
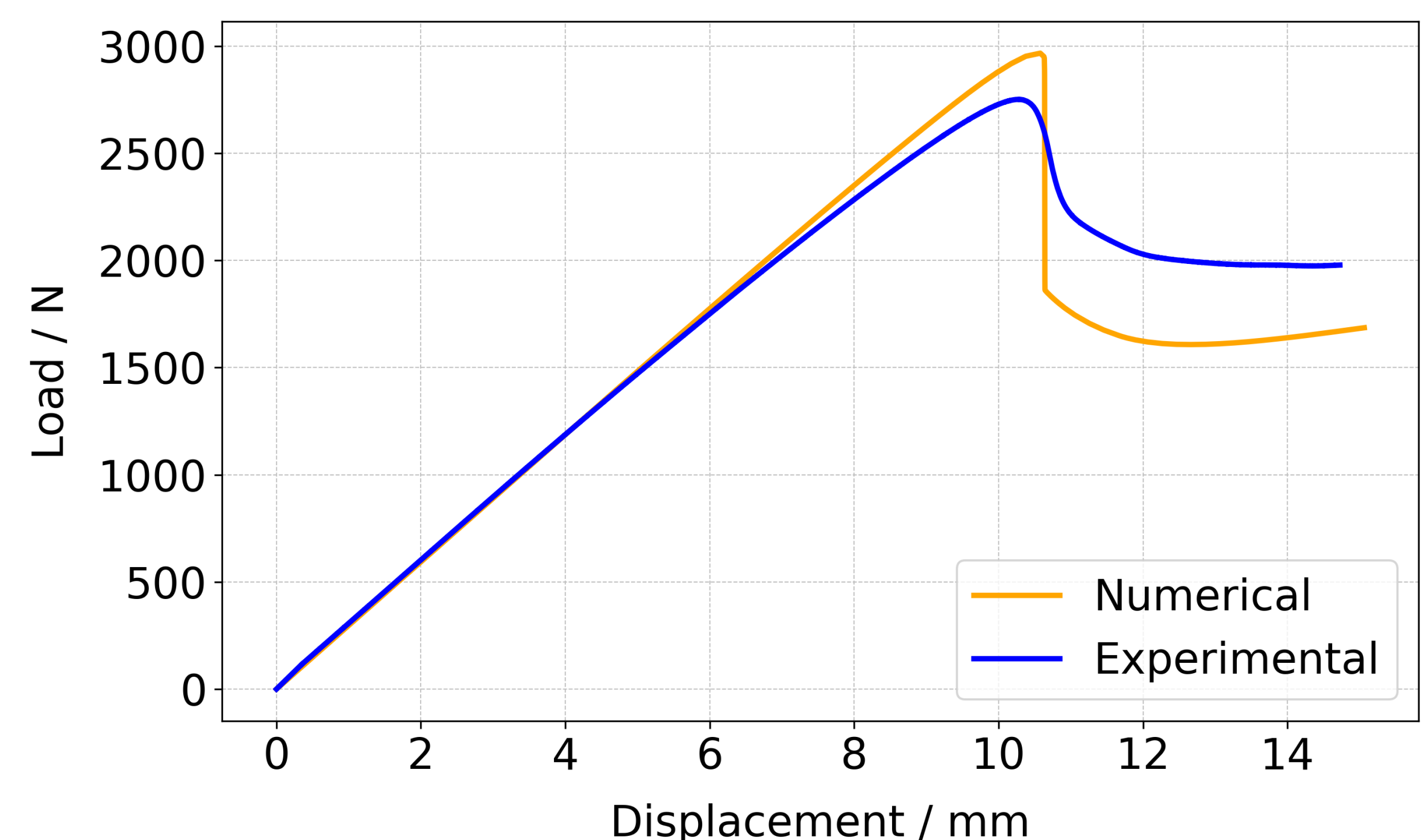
Figure 6 – Load-displacement curves for experimental and numerical results

Conclusions

In conclusion, this study successfully utilized the direct method to determine fracture properties in mode II of a structural adhesive using ENF specimens. The use of J-integral exhibited good repeatability and demonstrated strong agreement with CBBM results. Moreover, the cohesive law derived from the experimental data was employed to input a damage curve into a CZM model. The model accurately predicted that the FPZ reaches the middle roller, consistent with experimental observations. The close agreement between numerical and experimental results indicates the viability of this method for predicting adhesive fracture behavior in mode II.